



Deposited via The University of York.

White Rose Research Online URL for this paper:

<https://eprints.whiterose.ac.uk/id/eprint/203104/>

Version: Published Version

---

**Article:**

Mayhew, A. W., Edwards, P. M. and Hamilton, J. F. (2023) Daytime isoprene nitrates under changing NO<sub>x</sub> and O<sub>3</sub>. *Atmospheric Chemistry and Physics*. pp. 8473-8485. ISSN: 1680-7324

<https://doi.org/10.5194/acp-23-8473-2023>

---

**Reuse**

This article is distributed under the terms of the Creative Commons Attribution (CC BY) licence. This licence allows you to distribute, remix, tweak, and build upon the work, even commercially, as long as you credit the authors for the original work. More information and the full terms of the licence here:

<https://creativecommons.org/licenses/>

**Takedown**

If you consider content in White Rose Research Online to be in breach of UK law, please notify us by emailing [eprints@whiterose.ac.uk](mailto:eprints@whiterose.ac.uk) including the URL of the record and the reason for the withdrawal request.



## Daytime isoprene nitrates under changing $\text{NO}_x$ and $\text{O}_3$

Alfred W. Mayhew<sup>1</sup>, Peter M. Edwards<sup>1</sup>, and Jaqueline F. Hamilton<sup>1,2</sup>

<sup>1</sup>Wolfson Atmospheric Chemistry Laboratories, Department of Chemistry,  
University of York, Heslington, York, UK

<sup>2</sup>National Centre for Atmospheric Science, University of York, York, UK

**Correspondence:** Jaqueline F. Hamilton (jacqui.hamilton@york.ac.uk)

Received: 10 February 2023 – Discussion started: 21 February 2023

Revised: 22 June 2023 – Accepted: 26 June 2023 – Published: 31 July 2023

**Abstract.** Organonitrates are important species in the atmosphere due to their impacts on  $\text{NO}_x$ ,  $\text{HO}_x$ , and  $\text{O}_3$  budgets, and their potential to contribute to secondary organic aerosol (SOA) mass. This work presents a steady-state modelling approach to assess the impacts of changes in  $\text{NO}_x$  and  $\text{O}_3$  concentrations on the organonitrates produced from isoprene oxidation. The diverse formation pathways to isoprene organonitrates dictate the responses of different groups of organonitrates to changes in  $\text{O}_3$  and  $\text{NO}_x$ . For example, organonitrates predominantly formed from the OH-initiated oxidation of isoprene favour formation under lower-ozone and moderate- $\text{NO}_x$  concentrations, whereas organonitrates formed via daytime  $\text{NO}_3$  oxidation show the highest formation under high- $\text{O}_3$  concentrations with little dependence on  $\text{NO}_x$  concentrations. Investigating the response of total organonitrates reveals complex and nonlinear behaviour with implications that could inform expectations of changes to organonitrate concentrations as efforts are made to reduce  $\text{NO}_x$  and  $\text{O}_3$  concentrations, including a region of  $\text{NO}_x$ – $\text{O}_3$  space where total organonitrate concentration is relatively insensitive to changes in  $\text{NO}_x$  and  $\text{O}_3$ . These conclusions are further contextualised by estimating the volatility of the isoprene organonitrates revealing the potential for high concentrations of low-volatility species under high-ozone conditions.

### 1 Introduction

Organonitrates are important species in the atmosphere due to their impacts on  $\text{NO}_x$ ,  $\text{HO}_x$ , and  $\text{O}_3$  budgets through gas-phase chemistry (Emmerson and Evans, 2009; Bates and Jacob, 2019; Schwantes et al., 2019, 2020; Vasquez et al., 2020). Their relatively low volatility also results in the potential to form secondary organic aerosol (SOA) via condensation onto existing particles, and some organonitrates can undergo reactive uptake to the particle phase (Hallquist et al., 2009; Schwantes et al., 2019; Palmer et al., 2022). Isoprene organonitrates have been widely studied due to the large emissions of isoprene resulting in the relevance of isoprene chemistry to a range of environments around the globe (Guenther et al., 2006; Pye et al., 2015; Reeves et al., 2021; Tsiligiannis et al., 2022).

Isoprene hydroxynitrate (IHN) is widely studied due to its formation from OH oxidation in the presence of NO resulting in high concentrations during the daytime (Fig. 1) (Xiong

et al., 2015; Wennberg et al., 2018). IHN also has formation routes from oxidation with the nitrate radical ( $\text{NO}_3$ ). Other commonly studied isoprene mononitrates include isoprene carbonyl nitrate (ICN) and isoprene hydroperoxy nitrate (IPN). IPN forms through the initial  $\text{NO}_3$  oxidation of isoprene to form an isoprene nitrooxyperoxy radical ( $\text{INO}_2$ ). The reaction of  $\text{INO}_2$  with  $\text{HO}_2$  then forms IPN. ICN has a range of formation pathways initiated by OH and  $\text{NO}_3$  oxidation. Isoprene dinitrate (IDN) can also form from  $\text{INO}_2$  by its reaction with NO.

Isoprene epoxides, such as isoprene epoxydiols (IEPOX), have long been of interest due to their potential to contribute to SOA by reactive uptake to acidified particles (Paulot et al., 2009; Surratt et al., 2010). Later work outlined the similar SOA-forming properties for the nitrated epoxide, isoprene nitrooxyhydroxy epoxide (INHE), with the first proposed formation route to INHE involving the OH oxidation of IPN (Fig. 2) (Schwantes et al., 2015). Recent work aiming to improve the representation of isoprene  $\text{NO}_3$  chemistry

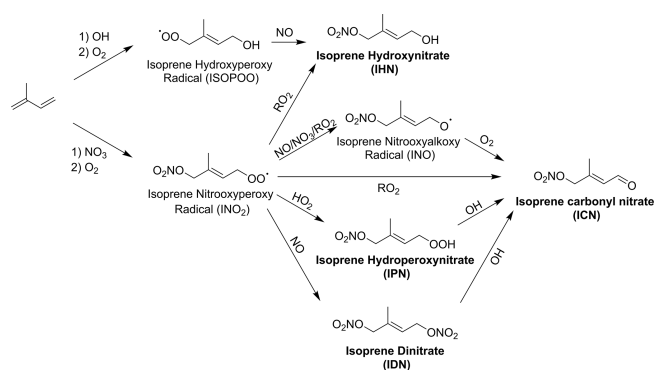


**Figure 1.** Formation routes to form IHN, ICN, IPN, and IDN from the OH- and NO<sub>3</sub>-initiated oxidation of isoprene. Additional isomers and reaction pathways have been omitted for clarity.

in chemical mechanisms highlighted a previously unrepresented reaction pathway to forming nitrated epoxides from alkoxy radicals (RO) (Vereecken et al., 2021; Carlsson et al., 2023). This alkoxy-epoxidation pathway provides an alternative formation route to INHE that does not rely on a stable intermediate or the presence of OH (Fig. 3). Additionally, three more nitrated epoxides can result from this pathway: isoprene nitrooxycarbonyl epoxide (INCE), isoprene nitrooxyhydroperoxy epoxide (INPE), and isoprene dinitrooxy epoxide (IDNE).

The motivation for the work presented here is based on findings from the 2017 Atmospheric Pollution and Human Health (APHH) in a Chinese Megacity summer campaign in Beijing, showing the role of NO<sub>3</sub> in the formation of isoprene organonitrates and their successive particle-phase products, including the afternoon period due to the presence of high-O<sub>3</sub> concentrations (Hamilton et al., 2021; Newland et al., 2021). The presence of high-O<sub>3</sub> concentrations increased the conversion of NO to NO<sub>2</sub> which subsequently reduced the loss of NO<sub>3</sub> to reaction with NO. Geyer (2003) first highlighted this in 2003, calculating daytime NO<sub>3</sub> mixing ratios of up to 2–5 ppt during the afternoon during a haze period in La Porte, Texas (Geyer, 2003). Since then, daytime NO<sub>3</sub> has been highlighted as a potentially important chemical pathway from a range of field campaigns in various cities around the world (Brown et al., 2005; Osthoff et al., 2006; Khan et al., 2015; Xue et al., 2016; Wang et al., 2020; Foulds et al., 2021). Daytime NO<sub>3</sub> chemistry has also been shown to be potentially significant under forest canopies, where photolytic processes are diminished (Forkel et al., 2006; Hu et al., 2013; Mermert et al., 2021).

The co-occurrence of organonitrate formation from OH and NO<sub>3</sub> chemistry, along with the multistage chemistry often required for their formation, results in the potential for complex dependencies on NO<sub>x</sub> and O<sub>3</sub> concentrations. However, these NO<sub>x</sub> and O<sub>3</sub> dependencies have not previously been investigated. This work describes efforts to investigate the sensitivity of daytime isoprene organonitrate chemistry

to changes in NO<sub>x</sub> and O<sub>3</sub> concentrations through a series of steady-state models. This work also aims to identify the role of O<sub>3</sub> concentrations in daytime NO<sub>3</sub> chemistry and determine the NO<sub>x</sub> and O<sub>3</sub> concentrations that facilitate this understudied reaction pathway. While the data presented here solely focus on nitrated species resulting from isoprene, similar variations in organonitrate speciation under different NO<sub>x</sub>–O<sub>3</sub> regimes are likely to hold for any volatile organic compound (VOC) which can undergo oxidation by both OH and NO<sub>3</sub> radicals.

## 2 Experimental

### 2.1 Model description

The goal of this work is to investigate changes in NO<sub>x</sub> and O<sub>3</sub> on the chemistry of isoprene nitrates in the afternoon period in Beijing. To do this, the models should demonstrate the favoured reaction pathways under different oxidant concentrations in the absence of other variables. This means that physical and photolytic processes should be held constant, i.e. the models will describe the chemistry occurring at a representative point in the day. Species must also be allowed to reach their steady-state concentrations in order to eliminate the role of the model spin-up period on resultant species concentrations. Comparison of the concentrations of species in these so-called steady-state models then allows for conclusions to be drawn as to the preferred oxidation products under various conditions.

All models described in this work were run using AtChem2, an open-source zero-dimensional box model (Sommariva et al., 2020). All models also made use of the isoprene mechanism published by Vereecken et al. (2021) (henceforth the FZJ mechanism) which aimed to improve the representation of NO<sub>3</sub> chemistry of isoprene by building on chemistry from the Master Chemical Mechanism (MCM) and the review of isoprene chemistry published by Wennberg et al. (2018) (Jenkin et al., 2015; Wennberg et al., 2018; Vereecken et al., 2021; Carlsson et al., 2023). In order to make the species naming consistent between the MCM portion and the added chemistry of the FZJ mechanism, ISOPCNO<sub>3</sub> was renamed to EISOP1N4OH as both identical species are present in the original FZJ mechanism.

The steady-state models are sets of models run at a range of fixed NO<sub>x</sub> and O<sub>3</sub> mixing ratios. Models were run for NO<sub>x</sub> mixing ratios up to 45 ppb and O<sub>3</sub> mixing ratios of 140 ppb, corresponding to the upper limit of measurements made in the Beijing 2017 campaign (Shi et al., 2019). In order to provide additional OH reactivity, a constant concentration of methane was added to all of the models to ensure that the modelled OH reactivity matched measured values under Beijing-like conditions; this is discussed further in the “Model Validation” section. The required mixing ratio corresponded to 82 ppm of methane in all of the models. The modelled concentration of species is taken as the final con-



of each plot to highlight the contour shape. These lines are equally spaced in the coloured dimension (e.g. species concentration), meaning close vertical lines would correspond to a strong sensitivity to changes in  $\text{O}_3$  and close horizontal lines would correspond to a strong sensitivity to changes in  $\text{NO}_x$ .

Under real-world conditions, the  $\text{O}_3$  concentrations will be determined by the nonlinear interactions of  $\text{NO}_x$  and VOCs, which is in contrast to the models where  $\text{NO}_x$ ,  $\text{O}_3$ , and VOCs are all constrained. This means that some sections of the model isopleths will be inaccessible. For example, some amount of  $\text{O}_3$  will form in the presence of  $\text{NO}_x$  and VOCs, so occupying the upper-left corner of the isopleths may not be possible outside of the constrained model scenario. Similarly, it may not be possible to map real-world changes to one dimension (such as a decrease in  $\text{NO}_x$ ) onto the isopleth plots without accounting for a change in the other dimension (such as a change in  $\text{O}_3$ ).

### 2.3 Volatility calculations

Section 3.6 makes use of the vapour pressure (often expressed as a log value to the base of 10) to investigate the potential contributions to SOA. The UManSysProp facility was used to do this (Topping et al., 2016); UManSysProp can estimate the vapour pressure of compounds represented as SMILES strings via a range of different group contribution methods (Barley and Mcfiggans, 2010; O'Meara et al., 2014). This work used predictions at 298 K throughout and used the “evaporation” technique, though sensitivity to all of the available prediction methods is described in Sect. 3.6.

## 3 Results and discussion

### 3.1 Model validation

As a test of the ability of the steady-state models to represent conditions present under ambient scenarios, the model results were compared to measurements collected in the summer of 2017 in Beijing (Shi et al., 2019; Hamilton et al., 2021; Whalley et al., 2021; Reeves et al., 2021; Newland et al., 2021; Mayhew et al., 2022). The  $\text{NO}_x$  mixing ratios measured in the afternoon periods in Beijing ranged between 5 and 20 ppb, and  $\text{O}_3$  mixing ratios ranged from around 60 to 140 ppb. Isoprene mixing ratios ranged up to around 2 ppb in the afternoon period, hence a typical value of 1 ppb was chosen for the steady-state models. The concentration isopleths for inorganic species that were zoomed in to this representative range of  $\text{O}_3$  and  $\text{NO}_x$  mixing ratios are provided in the Supplement (Sect. S1).

Measurements of OH reactivity ( $k_{\text{OH}}$ ) during the afternoon period were between around 10 and  $30 \text{ s}^{-1}$  (Whalley et al., 2021), which the models reproduced at the appropriate  $\text{NO}_x$  and  $\text{O}_3$  mixing ratios by design due to the additional methane included in the model run for this purpose (Fig. 4a). The

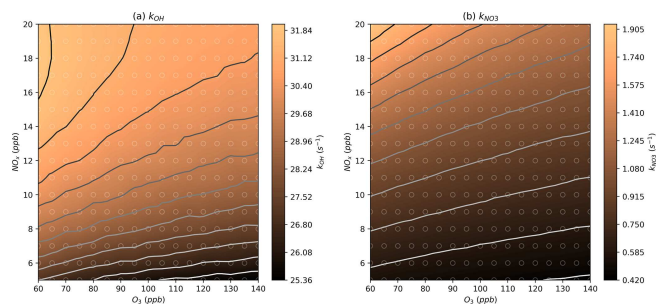


**Figure 4.** Modelled steady-state  $k_{\text{OH}}$  and  $k_{\text{NO}_3}$  values at different  $\text{NO}_x$  and  $\text{O}_3$  mixing ratios. Further details on interpreting these plots are given in Sect. 2.2.

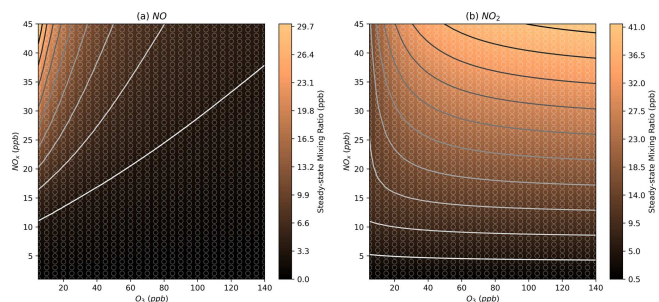


**Figure 5.** Modelled steady-state mixing ratios of NO and  $\text{NO}_2$  at different  $\text{NO}_x$  and  $\text{O}_3$  mixing ratios. Further details on interpreting these plots are given in Sect. 2.2.

modelled  $\text{NO}_3$  reactivity ( $k_{\text{NO}_3}$ ) is around  $0.4\text{--}1.9 \text{ s}^{-1}$  compared to the estimated value of around  $0.5 \text{ s}^{-1}$  presented in Hamilton et al. (2021) (Fig. 4b) (Hamilton et al., 2021). Values of  $k_{\text{OH}}$  and  $k_{\text{NO}_3}$  at a wider range of  $\text{NO}_x$  and  $\text{O}_3$  mixing ratios are provided in Fig. S1.

In the  $\text{NO}_x\text{--O}_3$  space corresponding to typical Beijing afternoon conditions, the models show NO mixing ratios of around  $0.3\text{--}2.8$  ppb (Figs. 5a, S2a), consistent with the low-NO observations in the afternoon period in Beijing with observed mixing ratios of around 0.25 and 3 ppb (Newland et al., 2021). The models show  $\text{NO}_3$  mixing ratios of 0.4 to 2 ppt (Figs. 6a, S3a), which are slightly below the measured  $\text{NO}_3$  mixing ratio in the afternoon of around 2 ppt (Hamilton et al., 2021). The modelled OH concentrations are between  $2.5 \times 10^6$  and  $6.5 \times 10^6$  molecules  $\text{cm}^{-3}$  (Figs. 6b, S3b), which are slightly below the measured concentrations of around  $7.5 \times 10^6$  molecules  $\text{cm}^{-3}$ .  $\text{HO}_2$  is generally overpredicted with a range between  $4.2 \times 10^8$  and  $9.1 \times 10^8$  molecules  $\text{cm}^{-3}$ , compared to measurements of around  $2.5 \times 10^8$  molecules  $\text{cm}^{-3}$  (Figs. 6c, S3c) (Whalley et al., 2021). This is consistent with previous modelling studies that indicate an overprediction of  $\text{HO}_2$  by models, particularly under the low-NO afternoon conditions being investigated here (Mayhew et al., 2022; Whalley et al., 2021). Furthermore, models that included an additional sink of  $\text{HO}_2$  to bring it in line with mea-

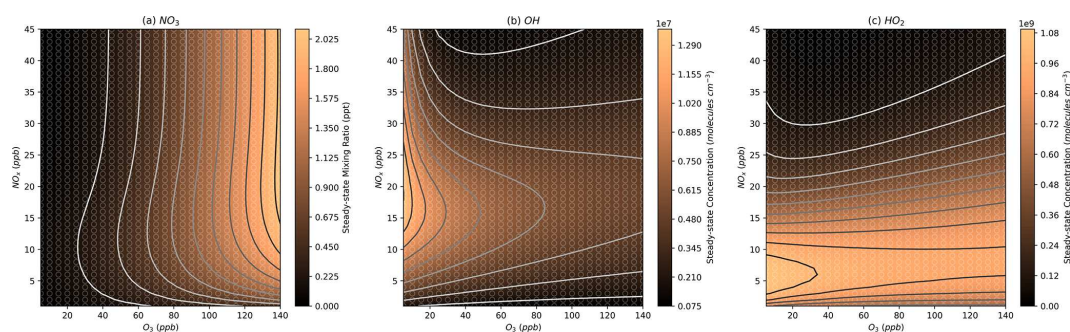


**Figure 6.** Modelled steady-state concentrations of  $\text{NO}_3$ ,  $\text{OH}$ , and  $\text{HO}_2$  at different  $\text{NO}_x$  and  $\text{O}_3$  mixing ratios. Further details on interpreting these plots are given in Sect. 2.2.

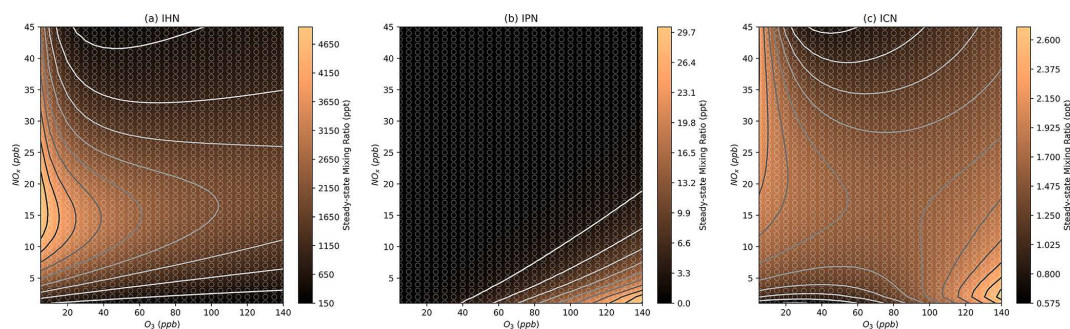


**Figure 7.** Modelled steady-state concentrations of isoprene hydroxynitrate (IHN), isoprene carbonylnitrate (ICN), and isoprene hydroperoxynitrate (IPN) at different  $\text{NO}_x$  and  $\text{O}_3$  mixing ratios. Further details on interpreting these plots are given in Sect. 2.2.

measurements resulted in an underprediction of  $\text{OH}$  due to the  $\text{HO}_x$  removed from the system.

A series of sensitivity tests were carried out in order to assess the sensitivity of our conclusions to changes in model parameters. Four different parameters were adjusted: the concentration of isoprene, the concentration of methane, the dilution rate, and the time of day. These sensitivity tests were found to have little impact on the conclusions drawn in this work, and any potential impacts are discussed where required. Further details on tests are provided in the Supplement (Sect. S2).

### 3.2 Mononitrates

The IHN concentration isopleth (Fig. 7a) shows a strong similarity to the  $\text{OH}$  isopleth (Fig. 6b), highlighting its rapid formation from the  $\text{OH}$  oxidation of isoprene and subsequent  $\text{RO}_2 + \text{NO}$  reaction to form the nitrate group (Fig. 1). This means that at high- $\text{O}_3$  mixing ratios, IHN shows a strong dependence on  $\text{NO}_x$ , and the dependence on  $\text{O}_3$  becomes more significant at lower- $\text{O}_3$  mixing ratios.

IPN shows increasing concentrations with increasing  $\text{O}_3$  and decreasing  $\text{NO}_x$  (Fig. 7b). This reflects the requirement for low- $\text{NO}$  concentrations to be present for two reasons. Firstly, high- $\text{NO}_3$  concentrations are required to form the  $\text{INO}_2$  radical by the reaction of isoprene with  $\text{NO}_3$ . Secondly,

the  $\text{RO}_2 + \text{HO}_2$  reaction is required to form the hydroperoxide group of IPN, and so lower- $\text{NO}$  concentrations will reduce competition with the rapid  $\text{RO}_2 + \text{NO}$  reaction. Additionally,  $\text{HO}_2$  concentrations are highest under low- $\text{NO}_x$  conditions (Fig. 6c), further favouring the  $\text{RO}_2 + \text{HO}_2$  reaction.

In contrast to the other nitrated species investigated here, ICN shows two peaks in concentration, one at very low  $\text{O}_3$  and the other at very high  $\text{O}_3$  (Fig. 7c). This is because ICN can be formed from many different routes. These routes include the abstraction of an H atom from IHN which provides a formation route under lower- $\text{O}_3$  conditions, when  $\text{OH}$  and IHN are both high in concentration. Alternatively, under higher- $\text{O}_3$  conditions, ICN can form from the reaction of  $\text{OH}$  and IPN or the decomposition of nitrated alkoxy radicals (INO). The result of these multiple peaks is that under moderate  $\text{NO}_x$  and  $\text{O}_3$  conditions, the concentration of ICN is relatively insensitive to changes in both  $\text{NO}_x$  and  $\text{O}_3$ . It is also important to note that the absolute concentrations of ICN predicted to form in these models are very low (the peaks in concentration corresponding to mixing ratios of just over 1 ppt) due to low production rates, which is consistent with low daytime ICN mixing ratios previously identified in Beijing (Reeves et al., 2021; Mayhew et al., 2022).

Recent work has highlighted species with the formula  $\text{C}_4\text{H}_7\text{NO}_5$  as potentially major oxidation products of iso-

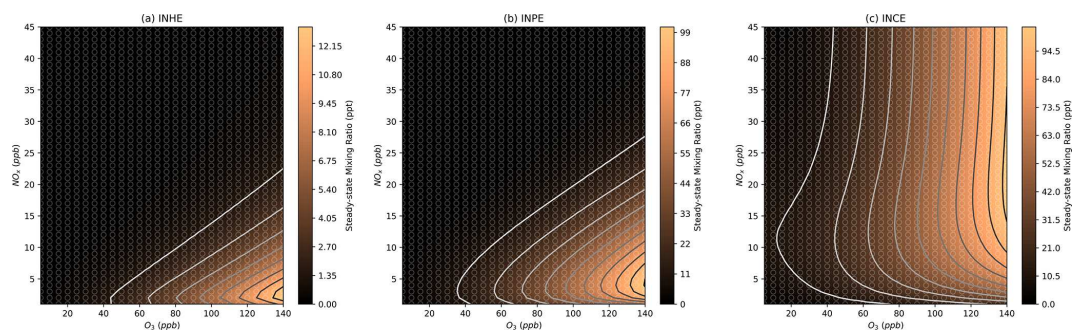


**Figure 8.** Modelled steady-state concentrations of isoprene hydroxynitrooxyepoxide (INHE), isoprene carbonylnitrooxyepoxide (INCE), and isoprene hydroperoxynitrooxyepoxide (INPE) at different  $\text{NO}_x$  and  $\text{O}_3$  mixing ratios. Further details on interpreting these plots are given in Sect. 2.2.

prene (Tsiligiannis et al., 2022). Consistent with previous modelling studies (Mayhew et al., 2022), these models largely form  $\text{C}_4\text{H}_7\text{NO}_5$  from OH-initiated oxidation, meaning the concentration isopleth is similar to that of OH and IHN.

### 3.3 Nitrated epoxides

Both INHE and INPE show a similar pattern as IPN in the  $\text{NO}_x$ – $\text{O}_3$  isopleths (Fig. 8a, b), with the highest concentrations occurring at low  $\text{NO}_x$  and very high  $\text{O}_3$ . INPE is reliant on high  $\text{NO}_3$  and  $\text{HO}_2$  in a similar manner to IPN as the  $\text{RO}_2 + \text{HO}_2$  step is still required to form INPE. While  $\text{HO}_2$  is not required to form INHE via the alkoxy-epoxidation pathway, the formation of INHE from IPN is the major formation route under lower- $\text{NO}_x$  conditions. Additionally, the alkoxy-epoxidation pathway to the formation of INHE relies on an  $\text{RO}_2$ – $\text{RO}_2$  cross reaction. This cross reaction will be favoured under low- $\text{NO}_x$ –high- $\text{O}_3$  conditions, where  $\text{NO}$  concentrations will be the lowest, meaning that the competition with the rapid  $\text{RO}_2$ – $\text{NO}$  reaction is minimal. This requirement for very high  $\text{O}_3$  and low  $\text{NO}_x$  means that we should expect very low concentrations of daytime INHE and INPE under typical urban conditions. This is consistent with modelling of Beijing which showed that while INHE may comprise a large fraction of nighttime  $\text{C}_5\text{H}_9\text{NO}_5$  compounds, the daytime contribution is very small (Mayhew et al., 2022).

In contrast, INCE shows reasonably high concentrations under high- $\text{O}_3$  mixing ratios at a range of  $\text{NO}_x$  mixing ratios. The profile of these concentrations is very similar to the  $\text{NO}_3$  isopleth (Fig. 6a) and stems from the main formation route to INCE requiring the  $\text{NO}_3$  oxidation of isoprene followed by an  $\text{RO}_2 + \text{NO}$  reaction step. This formation route shares similarities with the dinitrates discussed in Sect. 3.4.

### 3.4 Dinitrates

As previously noted for INCE, Fig. 9 shows that the steady-state concentrations of isoprene dinitrate (IDN) and isoprene

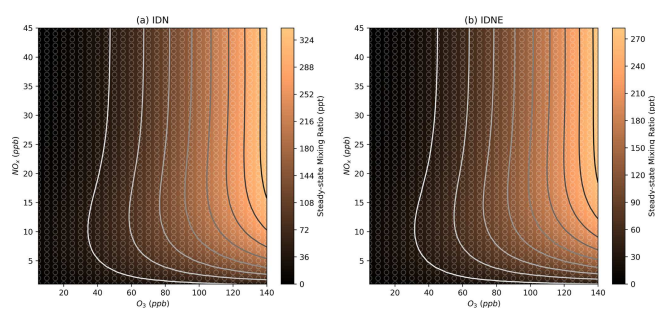


**Figure 9.** Modelled steady-state concentrations of isoprene dinitrate (IDN) and isoprene dinitrooxyepoxide (IDNE) at different  $\text{NO}_x$  and  $\text{O}_3$  mixing ratios. Further details on interpreting these plots are given in Sect. 2.2.

dinitrooxyepoxide (IDNE) are very similar to the  $\text{NO}_3$  concentration isopleth (Fig. 6a). This is indicative of the formation route of IDN and IDNE, where an initial  $\text{NO}_3$  oxidation is followed by the reaction of the resulting  $\text{RO}_2$  with  $\text{NO}$  to form the second nitrate group (Figs. 1 and 3). At any daytime concentration of  $\text{NO}_x$  where sufficient  $\text{NO}_3$  is present to perform the initial oxidation step, there will also be sufficient  $\text{NO}$  present to rapidly react with the resulting  $\text{RO}_2$ . Although the high- $\text{O}_3$  mixing ratios observed in Beijing result in low- $\text{NO}$  concentrations compared to typical daytime concentrations in a polluted megacity, there is still ample  $\text{NO}$  present to react with peroxy radicals produced by the initial  $\text{NO}_3$  oxidation. Figure 9 shows that at each  $\text{O}_3$ , there is a critical  $\text{NO}_x$  concentration above which the concentration of IDN, IDNE, and INCE is almost exclusively controlled by  $\text{O}_3$  concentrations. This critical  $\text{NO}_x$  mixing ratio is reasonably low compared to typical urban  $\text{NO}_x$  mixing ratios, indicating that the concentration of dinitrates in urban environments may be largely controlled by the  $\text{O}_3$  mixing ratios present.

As discussed in Sect. S2, increasing the total VOC in the model leads to a broadening in the  $\text{NO}_x$  axis of the transition between sensitive regimes of  $\text{NO}_x$  and  $\text{O}_3$  for  $\text{NO}_3$ ; the same also applies to IDN, IDNE, and INCE. For a fixed ozone con-

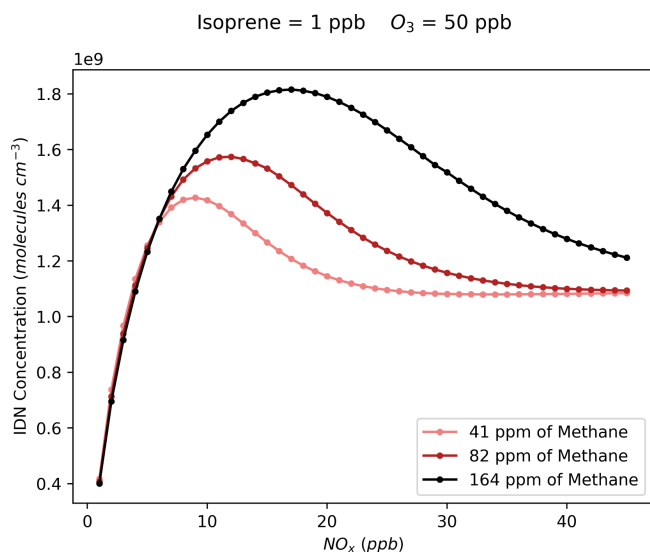


**Figure 10.** Modelled steady-state concentrations of IDN with changing NO<sub>x</sub> in models runs with 50 ppb of O<sub>3</sub> and different mixing ratios of NO<sub>x</sub> and additional methane.

centration, increasing the NO<sub>x</sub> from 0 will increase IDN, IDNE, or INCE concentrations due to the increased NO<sub>3</sub> resulting from the increased availability of NO<sub>2</sub> (Fig. 10). Then, once the threshold NO<sub>x</sub> concentration is reached and NO<sub>3</sub> concentrations are not limited by the availability of NO<sub>x</sub>, the concentration becomes controlled by O<sub>3</sub> and HO<sub>2</sub> (Sect. S2), creating the “hump” in concentration which then stabilises as HO<sub>2</sub> concentrations begin to decrease at high NO<sub>x</sub> and the NO<sub>2</sub>/NO ratio becomes increasingly controlled by the fixed O<sub>3</sub> concentration. This means that with high-VOC concentrations, at a given O<sub>3</sub> concentration, reductions in NO<sub>x</sub> will result in increased IDN, IDNE, or ICNE concentrations sooner than under lower-VOC conditions.

### 3.5 Total organonitrates

By summing the model concentrations for all organonitrates present in the mechanism, an isopleth of total organonitrates was obtained (Fig. 11). This shows a band of high-organonitrate concentrations at moderate NO<sub>x</sub>. At high O<sub>3</sub>, further changes to O<sub>3</sub> have little effect on the total organonitrate concentration. Total organonitrates also become less sensitive to changes in NO<sub>x</sub> in this high-O<sub>3</sub> region. This band is the result of organonitrates produced by OH and NO<sub>3</sub> oxidation of isoprene. At low-O<sub>3</sub> mixing ratios, the total organonitrates are dominated by OH-initiated species such as IHN (Fig. 7a). Conversely, at high-O<sub>3</sub> mixing ratios, NO<sub>3</sub>-initiated species such as IDN comprise a larger fraction of total organonitrates (Fig. 9a). This is illustrated in the pie charts in Fig. 11 which show the organonitrate composition under different NO<sub>x</sub>–O<sub>3</sub> regimes.

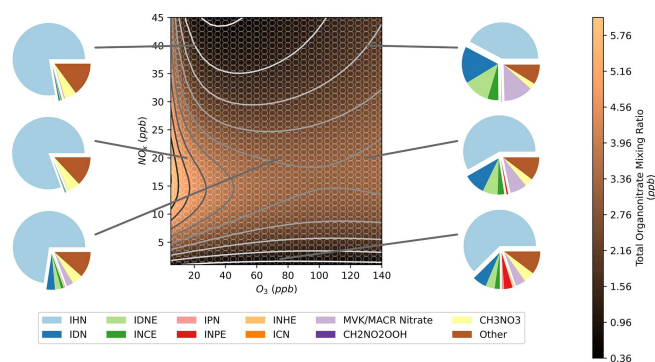


**Figure 11.** Modelled steady-state concentrations of the total organonitrates at different NO<sub>x</sub> and O<sub>3</sub> mixing ratios along with the composition of the total organonitrates at selected NO<sub>x</sub> and O<sub>3</sub> mixing ratios. Further details on interpreting these plots are given in Sect. 2.2.

The composition breakdown also reveals that total isoprene organonitrates are dominated by IHN under most conditions, but this fraction decreases as ozone mixing ratios increase. At higher O<sub>3</sub>, a large fraction of the composition comes from IDN, IDNE, and INCE due to their higher concentrations under high-O<sub>3</sub> conditions (Sect. 3.3 and 3.4). CH<sub>3</sub>NO<sub>3</sub> comprises a substantial fraction of total organonitrates in these models. CH<sub>3</sub>NO<sub>3</sub> can be formed by the OH oxidation of methane via the methylperoxy radical, and so its concentrations in these models are exaggerated due to the large amounts of methane added to the model. Formation from the OH oxidation of methane comprises the majority of all of the methylperoxy formation in all of the models, excluding formation from the reversible decomposition of methane peroxyxynitrate (CH<sub>3</sub>O<sub>2</sub>NO<sub>2</sub>) which is balanced by the opposing formation reaction. CH<sub>2</sub>NO<sub>2</sub>OOH is also listed in Fig. 11. CH<sub>2</sub>NO<sub>2</sub>OOH is formed from the products of isoprene ozonolysis, explaining the higher concentrations under high-O<sub>3</sub> conditions. There are no chemical losses in the mechanism for CH<sub>2</sub>NO<sub>2</sub>OOH, which likely explains the high contribution to total organonitrates. The remaining portion of “other” organonitrates corresponds to a wide range of species, none of which contribute more than 6% to the total organonitrate sum in any models.

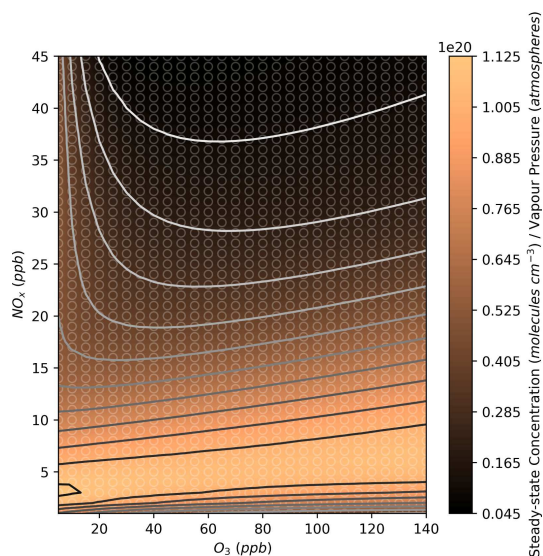
As noted in Sect. S2, changing the VOC concentration affects the position in NO<sub>x</sub>–O<sub>3</sub> space where the maximum organonitrate concentrations are observed. In the case of total organonitrates, decreasing the total VOC concentration results in the band of high concentrations moving to lower NO<sub>x</sub>. Figures S7 and S8 show that with lower-methane concentrations in the model, the peak organonitrate concentrations occur at around 12 ppb of NO<sub>x</sub> whereas this increases to around 25 ppb of NO<sub>x</sub> in the high-methane case. The peak organonitrate concentrations at each of these NO<sub>x</sub> concentrations are similar in each of these sets of model runs.

### 3.6 Volatility assessment

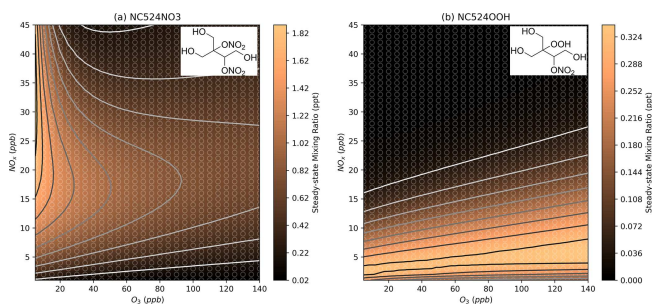
One of the major motivations for studying isoprene nitrates is their potential to contribute to secondary organic aerosol (SOA) by condensation or reactive uptake to existing particles. While the highest concentration species such as IHN and IDN may be most significant when considering the role of isoprene nitrates as NO<sub>x</sub> reservoirs, low-concentration species can be much more important for SOA formation if they are of a sufficiently low volatility. As an estimation of the impact of changing NO<sub>x</sub> and O<sub>3</sub> on particle-phase processes, the log of the vapour pressure was estimated for each organonitrate in the mechanism based on the species' structure using UManSysProp (Topping et al., 2016). As a measure of a compound's volatility, a lower vapour pressure value corresponds to a less volatile compound which will more readily partition into existing particles. This volatility-based approach does not account for potential reactive uptake, which is likely to be important for the epoxide species previously discussed. Furthermore, the hydrolysis of organonitrates, particularly tertiary nitrates, may reduce particle-phase concentrations (Vasquez et al., 2020). This particle-phase hydrolysis may then have knock-on effects for the gas-phase organonitrates, particularly where the tertiary nitrate isomer comprises a large fraction of the composition, such as for IHN.

Figure 12 shows the total organonitrate plot normalised to the vapour pressure value for each compound, which gives an estimation of the contribution of organonitrate uptake to SOA at each NO<sub>x</sub> and O<sub>3</sub> mixing ratio. Since the predicted vapour pressures range over 10 orders of magnitude, lower-volatility species can have a large effect on SOA formation despite their much lower concentration. The lowest vapour pressures predicted here are for the two MCM species NC524NO<sub>3</sub> and NC524OOH. These two compounds comprise almost 100 % of the normalised concentration in Fig. 12 under all NO<sub>x</sub> and O<sub>3</sub> conditions, and their individual concentration profiles can be seen in Fig. 13. The concentration isopleths for the 15 lowest volatility compounds are shown in Fig. S17. Many of these species show profiles similar to that of NC524OOH, with the highest concentrations occurring at low urban NO<sub>x</sub> concentrations.

According to Fig. 12, reductions in NO<sub>x</sub> from typical urban conditions would result in higher normalised concentrations of organonitrates, meaning the contribution of isoprene nitrates to SOA may increase with decreasing NO<sub>x</sub> until very low urban NO<sub>x</sub> conditions are met. However, it is important to note the difficulty in representing the lowest-volatility species in the isoprene oxidation mechanism. Many of these species are the product of multiple oxidation steps with large uncertainties surrounding their rates of formation. Additionally, many of the lowest-volatility species do not contain any chemical losses in the mechanism due to a lack of information on their reactions.



**Figure 12.** Modelled steady-state concentrations of the total organonitrates normalised to each compound's estimated vapour pressure at different NO<sub>x</sub> and O<sub>3</sub> mixing ratios. Further details on interpreting these plots are given in Sect. 2.2.



**Figure 13.** Modelled steady-state concentrations of the MCM species NC524NO<sub>3</sub> and NC524OOH at different NO<sub>x</sub> and O<sub>3</sub> mixing ratios. Further details on interpreting these plots are given in Sect. 2.2.

The low predicted volatilities of NC524NO<sub>3</sub> and NC524OOH are the result of the many functional groups present in the molecules. Similarly, oxidised species could be described as highly oxidised molecules (HOMs) (Bianchi et al., 2019). The chemistry of HOMs is not currently well represented in many mechanisms due to their varied autoxidation formation pathways. For example, the profile of NC524OOH concentrations in Fig. 13b results from the requirement of HO<sub>2</sub> to form the hydroperoxide group, hence the profile is similar to that of HO<sub>2</sub>. If an RO<sub>2</sub> H-shift formation pathway to NC524OOH, or similar HOMs, were included in the mechanism, then this might alter the profile in Fig. 12 (Vereecken and Nozière, 2020). It should be expected that the formation of HOMs would be sensitive to changes in ozone as the lower-NO concentrations at higher ozone will reduce the competition of the RO<sub>2</sub>+NO path-

way with the RO<sub>2</sub> autoxidation reactions that form HOMs. Inclusion of improved autoxidation chemistry in the mechanisms would also increase the number of low-volatility compounds produced from the oxidation of isoprene. There is also the potential for the oxidation products of nighttime species to be low-volatility compounds that would contribute to SOA but would not be captured by these models which represent the steady-state concentration of organonitrates at 16:00 LT, without the contribution of chemistry occurring at other times of the day.

Figure S16 shows that the results presented here are reasonably insensitive to the choice of vapour pressure and boiling point prediction methods selected within UManSysProp. Section S3 also outlines the results using an alternative volatility estimation method, making use of only the molecular formula of each compound.

### 3.7 Application to less polluted environments

In order to test the investigation of less polluted environments, a series of models were run at a range of lower-NO<sub>x</sub> and lower-O<sub>3</sub> mixing ratios. Measurements collected in the Amazon rainforest were taken as an example of an unpolluted environment, and the model was adjusted to match typical isoprene mixing ratios and OH reactivity observed in this environment. The results from these models are presented in the supplementary information (Sect. S5).

The reduced NO<sub>x</sub> and O<sub>3</sub> mixing ratios used in these models mean that, despite the changes to isoprene and methane concentrations, they correspond well to higher-resolution models of the low-NO<sub>x</sub> and low-O<sub>3</sub> portions of the Beijing models. Figure S19 shows that the total organonitrates in the Amazon models are sensitive to changes in NO<sub>x</sub>, with increasing ozone slightly reducing total organonitrates.

As discussed in the introduction, IEPOX is one of the major precursors of isoprene SOA, particularly under low-NO<sub>x</sub> conditions where the IEPOX precursor, ISOPOOH, can form from oxidation by OH and further reaction with HO<sub>2</sub>. This dependence on HO<sub>2</sub> means that the Amazon models predict increasing concentrations of IEPOX as NO<sub>x</sub> is increased from close to 0, regardless of the O<sub>3</sub> concentration (Fig. 14b). This is in agreement with findings from Shrivastava et al. who found increases in isoprene SOA resulting from increases in NO<sub>x</sub> and O<sub>3</sub> from an urban plume (Shrivastava et al., 2019). The increased SOA could be further explained by the increases in nitrated epoxides and dinitrated species predicted on increasing both NO<sub>x</sub> and O<sub>3</sub> (Fig. S19).

Methyl vinyl ketone (MVK) and methacrolein (MACR) are also often of interest in isoprene oxidation, particularly in pristine environments such as the Amazon where the production of MVK and MACR relies on the presence of NO (Langford et al., 2022). This is illustrated in Fig. 14d, whereas Fig. 14c illustrates that the abundance of NO under typical urban conditions means that the MVK + MACR concentra-

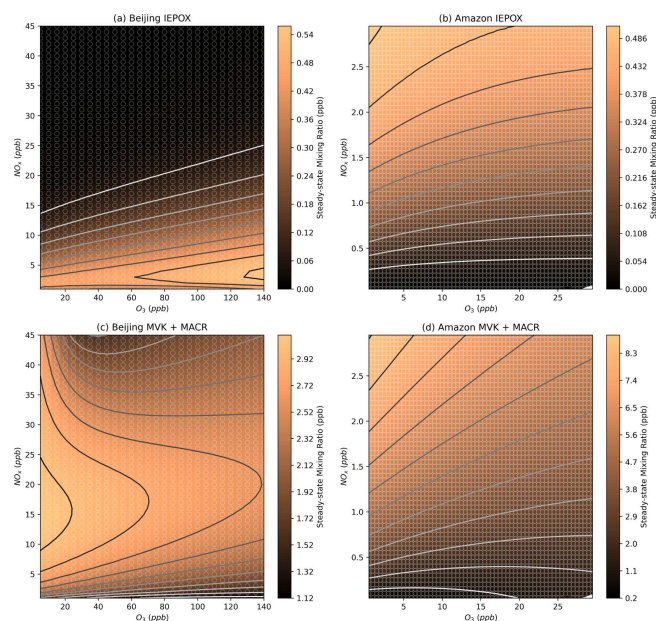


**Figure 14.** Modelled steady-state IEPOX and MVK + MACR concentrations for the Beijing (a, c) and Amazon (b, d) models.

tions in the Beijing models are dependent on OH concentrations.

## 4 Conclusions

The work presented here illustrates that each isoprene nitrate species will have a different NO<sub>x</sub>–O<sub>3</sub> regime in which maximum concentrations will be produced during the afternoon period. For example, the facile formation of IHN from OH oxidation means that daytime concentrations are largely dictated by the concentration of OH. Alternatively, the concentrations of species such as IDN, IDNE, and ICN are largely dictated by the available daytime NO<sub>3</sub> as the reaction of RO<sub>2</sub> with NO is very rapid, even under low urban NO<sub>x</sub> conditions. Finally, IPN, INHE, and INPE only show the highest concentrations under low-NO<sub>x</sub>–high-O<sub>3</sub> conditions due to their increased formation under high-NO<sub>3</sub> concentrations and their requirement for low NO<sub>x</sub> to avoid competition with the RO<sub>2</sub>+NO reaction pathway.

The fact that the concentrations of different organonitrates will respond differently to changes in NO<sub>x</sub> and O<sub>3</sub> will have implications for those considering pathways to reducing the concentrations of organonitrates in the atmosphere. The work presented here indicates that reductions in NO<sub>x</sub> may not reduce total organonitrate concentrations until low urban NO<sub>x</sub> conditions are met and that, for many of the species resulting from the daytime NO<sub>3</sub> oxidation of isoprene, organonitrate concentrations may be much more sensitive to changes in O<sub>3</sub> than in NO<sub>x</sub>. Additionally, accounting for the volatility of the organonitrates can have very large impacts, and the models presented here are dominated by a small num-

ber of low-volatility compounds. An improved representation of late-stage oxidation and autoxidation is likely to improve the ability to predict the effect of changing O<sub>3</sub> and NO<sub>x</sub> on SOA formation. It is important to note that the simplified models presented here represent the formation of daytime isoprene organonitrates at 16:00 LT and will not capture the effect of organonitrates produced during the nighttime or those produced from the oxidation of nighttime products or other VOCs.

As efforts are made to reduce NO<sub>x</sub>, VOC, and O<sub>3</sub> concentrations around the world, care should be taken to ensure that the nonlinearity of responses to changes does not result in unintended increases in important SOA precursors. For example, previous work has indicated that Beijing occupies a VOC-limited regime with respect to O<sub>3</sub> formation and that decreasing NO<sub>x</sub> concentrations without a concurrent decrease in VOC concentrations would result in increased O<sub>3</sub> (Wei et al., 2019; Ren et al., 2021). Figure 12 suggests that many of the lowest-volatility daytime isoprene organonitrates may form in higher concentrations under higher O<sub>3</sub> and lower NO<sub>x</sub>. Furthermore, INHE, IDNE, INPE, and INCE all favour formation under high-O<sub>3</sub> conditions and may be subject to reactive uptake to the particle phase. This may be further compounded or mitigated with changing VOC concentrations due to the impact on the organonitrate isopleths as well as the nonlinear behaviour of O<sub>3</sub> with changing NO<sub>x</sub> and VOC.

Future chamber and field studies could validate the findings from this work by making more comprehensive observations of total and speciated organonitrates under different NO<sub>x</sub>, O<sub>3</sub>, and VOC concentrations. The comparative nature of these isopleth plots mean that the organonitrate measurement would not necessarily need to be calibrated, provided that the instrument response to specific organonitrates can be assumed to be constant. This makes long-term measurements made with chemical ionisation mass spectrometry (CIMS) a promising dataset as various CIMS techniques using a range of reagent ions (including I<sup>-</sup>, Br<sup>-</sup>, and CF<sub>3</sub>O<sup>-</sup>) have been shown to be very sensitive to these multifunctional compounds, but calibration is often difficult (Mayhew et al., 2022; Lee et al., 2014; Schwantes et al., 2019; Carlsson et al., 2023).

**Code availability.** The AtChem2 software used for modeling is open source and freely available via <https://github.com/AtChem> (AtChem, 2023; <https://doi.org/10.5194/gmd-13-169-2020>, Sommariva et al., 2020).

**Data availability.** No data sets were used in this article.

**Supplement.** The supplement related to this article is available online at: <https://doi.org/10.5194/acp-23-8473-2023-supplement>.

**Author contributions.** AWM performed the model simulations and prepared the paper. PME and JFH provided supervision and advice throughout the project.

**Competing interests.** The contact author has declared that none of the authors has any competing interests.

**Disclaimer.** Publisher's note: Copernicus Publications remains neutral with regard to jurisdictional claims in published maps and institutional affiliations.

**Acknowledgements.** This project was undertaken on the Viking Cluster, which is a high-performance compute facility provided by the University of York. We are grateful for computational support from the University of York High Performance Computing service, Viking and the Research Computing team.

**Financial support.** This work has been supported by the Leeds–York–Hull Natural Environment Research Council (NERC) Doctoral Training Partnership (DTP) Panorama (grant no. NE/S007458/1).

**Review statement.** This paper was edited by Steven Brown and reviewed by two anonymous referees.

## References

- AtChem: Popular repositories, GitHub [code], <https://github.com/AtChem> (last access: 21 February 2023), 2023.
- Barley, M. H. and McFiggans, G.: The critical assessment of vapour pressure estimation methods for use in modelling the formation of atmospheric organic aerosol, *Atmos. Chem. Phys.*, 10, 749–767, <https://doi.org/10.5194/acp-10-749-2010>, 2010.
- Bates, K. H. and Jacob, D. J.: A new model mechanism for atmospheric oxidation of isoprene: global effects on oxidants, nitrogen oxides, organic products, and secondary organic aerosol, *Atmos. Chem. Phys.*, 19, 9613–9640, <https://doi.org/10.5194/acp-19-9613-2019>, 2019.
- Bianchi, F., Kurtén, T., Riva, M., Mohr, C., Rissanen, M. P., Roldin, P., Berndt, T., Crouse, J. D., Wennberg, P. O., Mentel, T. F., Wildt, J., Junninen, H., Jokinen, T., Kulmala, M., Worsnop, D. R., Thornton, J. A., Donahue, N., Kjaergaard, H. G., and Ehn, M.: Highly Oxygenated Organic Molecules (HOM) from Gas-Phase Autoxidation Involving Peroxy Radicals: A Key Contributor to Atmospheric Aerosol, *Chem. Rev.*, 119, 3472–3509, <https://doi.org/10.1021/acs.chemrev.8b00395>, 2019.
- Brown, S. S., Osthoff, H. D., Stark, H., Dubé, W. P., Ryerson, T. B., Warneke, C., de Gouw, J. A., Wollny, A. G., Parrish, D. D., Fehsenfeld, F. C., and Ravishankara, A. R.: Aircraft observations of daytime NO<sub>3</sub> and N<sub>2</sub>O<sub>5</sub> and their implications for tropospheric chemistry, *J. Photoch. Photobio. A*, 176, 270–278, <https://doi.org/10.1016/j.jphotochem.2005.10.004>, 2005.

- Carlsson, P. T. M., Vereecken, L., Novelli, A., Bernard, F., Brown, S. S., Brownwood, B., Cho, C., Crowley, J. N., Dewald, P., Edwards, P. M., Friedrich, N., Fry, J. L., Hallquist, M., Hantschke, L., Hohaus, T., Kang, S., Liebmann, J., Mayhew, A. W., Mentel, T., Reimer, D., Rohrer, F., Shenolikar, J., Tillmann, R., Tsiligiannis, E., Wu, R., Wahner, A., Kiendler-Scharr, A., and Fuchs, H.: Comparison of isoprene chemical mechanisms under atmospheric night-time conditions in chamber experiments: evidence of hydroperoxy aldehydes and epoxy products from NO<sub>3</sub> oxidation, *Atmos. Chem. Phys.*, 23, 3147–3180, <https://doi.org/10.5194/acp-23-3147-2023>, 2023.
- Edwards, P. M., Young, C. J., Aikin, K., deGouw, J., Dubé, W. P., Geiger, F., Gilman, J., Helmig, D., Holloway, J. S., Kercher, J., Lerner, B., Martin, R., McLaren, R., Parrish, D. D., Peischl, J., Roberts, J. M., Ryerson, T. B., Thornton, J., Warneke, C., Williams, E. J., and Brown, S. S.: Ozone photochemistry in an oil and natural gas extraction region during winter: simulations of a snow-free season in the Uintah Basin, Utah, *Atmos. Chem. Phys.*, 13, 8955–8971, <https://doi.org/10.5194/acp-13-8955-2013>, 2013.
- Edwards, P. M., Brown, S. S., Roberts, J. M., Ahmadov, R., Banta, R. M., Degouw, J. A., Dubé, W. P., Field, R. A., Flynn, J. H., Gilman, J. B., Graus, M., Helmig, D., Koss, A., Langford, A. O., Lefer, B. L., Lerner, B. M., Li, R., Li, S.-M., McKeen, S. A., Murphy, S. M., Parrish, D. D., Senff, C. J., Soltis, J., Stutz, J., Sweeney, C., Thompson, C. R., Trainer, M. K., Tsai, C., Veres, P. R., Washenfelder, R. A., Warneke, C., Wild, R. J., Young, C. J., Yuan, B., and Zamora, R.: High winter ozone pollution from carbonyl photolysis in an oil and gas basin, *Nature*, 514, 351–354, <https://doi.org/10.1038/nature13767>, 2014.
- Emmerson, K. M. and Evans, M. J.: Comparison of tropospheric gas-phase chemistry schemes for use within global models, *Atmos. Chem. Phys.*, 9, 1831–1845, <https://doi.org/10.5194/acp-9-1831-2009>, 2009.
- Forkel, R., Klemm, O., Graus, M., Rappenglück, B., Stockwell, W. R., Grabmer, W., Held, A., Hansel, A., and Steinbrecher, R.: Trace gas exchange and gas phase chemistry in a Norway spruce forest: A study with a coupled 1-dimensional canopy atmospheric chemistry emission model, *Atmos. Environ.*, 40, 28–42, <https://doi.org/10.1016/j.atmosenv.2005.11.070>, 2006.
- Foulds, A., Khan, M. A. H., Bannan, T. J., Percival, C. J., Lowenberg, M. H., and Shallcross, D. E.: Abundance of NO<sub>3</sub> Derived Organo-Nitrates and Their Importance in the Atmosphere, *Atmosphere*, 12, 1381, <https://doi.org/10.3390/atmos12111381>, 2021.
- Geyer, A.: Direct observations of daytime NO<sub>3</sub>: Implications for urban boundary layer chemistry, *J. Geophys. Res.*, 108, 4368, <https://doi.org/10.1029/2002jd002967>, 2003.
- Guenther, A., Karl, T., Harley, P., Wiedinmyer, C., Palmer, P. I., and Geron, C.: Estimates of global terrestrial isoprene emissions using MEGAN (Model of Emissions of Gases and Aerosols from Nature), *Atmos. Chem. Phys.*, 6, 3181–3210, <https://doi.org/10.5194/acp-6-3181-2006>, 2006.
- Hallquist, M., Wenger, J. C., Baltensperger, U., Rudich, Y., Simpson, D., Claeys, M., Dommen, J., Donahue, N. M., George, C., Goldstein, A. H., Hamilton, J. F., Herrmann, H., Hoffmann, T., Iinuma, Y., Jang, M., Jenkin, M. E., Jimenez, J. L., Kiendler-Scharr, A., Maenhaut, W., McFiggans, G., Mentel, Th. F., Monod, A., Prévôt, A. S. H., Seinfeld, J. H., Surratt, J. D., Szmigielski, R., and Wildt, J.: The formation, properties and impact of secondary organic aerosol: current and emerging issues, *Atmos. Chem. Phys.*, 9, 5155–5236, <https://doi.org/10.5194/acp-9-5155-2009>, 2009.
- Hamilton, J. F., Bryant, D. J., Edwards, P. M., Ouyang, B., Bannan, T. J., Mehra, A., Mayhew, A. W., Hopkins, J. R., Dunmore, R. E., Squires, F. A., Lee, J. D., Newland, M. J., Worrall, S. D., Bacak, A., Coe, H., Percival, C., Whalley, L. K., Heard, D. E., Slater, E. J., Jones, R. L., Cui, T., Surratt, J. D., Reeves, C. E., Mills, G. P., Grimmond, S., Sun, Y., Xu, W., Shi, Z., and Rickard, A. R.: Key Role of NO<sub>3</sub> Radicals in the Production of Isoprene Nitrates and Nitrooxyorganosulfates in Beijing, *Environ. Sci. Technol.*, 55, 842–853, <https://doi.org/10.1021/acs.est.0c05689>, 2021.
- Hu, X.-M., Fuentes, J. D., Toohey, D., and Wang, D.: Chemical processing within and above a loblolly pine forest in North Carolina, USA, *J. Atmos. Chem.*, 72, 235–259, <https://doi.org/10.1007/s10874-013-9276-3>, 2013.
- Jenkin, M. E., Young, J. C., and Rickard, A. R.: The MCM v3.3.1 degradation scheme for isoprene, *Atmos. Chem. Phys.*, 15, 11433–11459, <https://doi.org/10.5194/acp-15-11433-2015>, 2015.
- Kenagy, H. S., Sparks, T. L., Wooldridge, P. J., Weinheimer, A. J., Ryerson, T. B., Blake, D. R., Hornbrook, R. S., Apel, E. C., and Cohen, R. C.: Evidence of Nighttime Production of Organic Nitrates During SEAC 4 RS, FRAPPÉ, and KORUS-AQ, *Geophys. Res. Lett.*, 47, e2020GL087860, <https://doi.org/10.1029/2020gl087860>, 2020.
- Khan, M. A. H., Morris, W. C., Watson, L. A., Galloway, M., Hamer, P. D., Shallcross, B. M. A., Percival, C. J., and Shallcross, D. E.: Estimation of Daytime NO<sub>3</sub> Radical Levels in the UK Urban Atmosphere Using the Steady State Approximation Method, *Adv. Meteorol.*, 2015, 1–9, <https://doi.org/10.1155/2015/294069>, 2015.
- Langford, B., House, E., Valach, A., Hewitt, C. N., Artaxo, P., Barkley, M. P., Brito, J., Carnell, E., Davison, B., MacKenzie, A. R., Marais, E. A., Newland, M. J., Rickard, A. R., Shaw, M. D., Yáñez-Serrano, A. M., and Nemitz, E.: Seasonality of isoprene emissions and oxidation products above the remote Amazon, *Environ. Sci.-Atmos.*, 2, 230–240, <https://doi.org/10.1039/d1ea00057h>, 2022.
- Lee, B. H., Lopez-Hilfiker, F. D., Mohr, C., Kurtén, T., Worsnop, D. R., and Thornton, J. A.: An Iodide-Adduct High-Resolution Time-of-Flight Chemical-Ionization Mass Spectrometer: Application to Atmospheric Inorganic and Organic Compounds, *Environ. Sci. Technol.*, 48, 6309–6317, <https://doi.org/10.1021/es500362a>, 2014.
- Mayhew, A. W., Lee, B. H., Thornton, J. A., Bannan, T. J., Brean, J., Hopkins, J. R., Lee, J. D., Nelson, B. S., Percival, C., Rickard, A. R., Shaw, M. D., Edwards, P. M., and Hamilton, J. F.: Evaluation of isoprene nitrate chemistry in detailed chemical mechanisms, *Atmos. Chem. Phys.*, 22, 14783–14798, <https://doi.org/10.5194/acp-22-14783-2022>, 2022.
- Mermet, K., Perraudin, E., Dusanter, S., Sauvage, S., Leonardis, T., Flaud, P. M., Bsaibes, S., Kammer, J., Michoud, V., Gratien, A., Cirtog, M., Al Ajami, M., Truong, F., Batut, S., Hecquet, C., Doussin, J. F., Schoemaeker, C., Gros, V., Locoge, N., and Villenave, E.: Atmospheric reactivity of biogenic volatile organic compounds in a maritime pine forest during the LANDEX episode 1 field campaign, *Sci. Total Environ.*, 756, 144129, <https://doi.org/10.1016/j.scitotenv.2020.144129>, 2021.

- Newland, M. J., Bryant, D. J., Dunmore, R. E., Bannan, T. J., Acton, W. J. F., Langford, B., Hopkins, J. R., Squires, F. A., Dixon, W., Drysdale, W. S., Ivatt, P. D., Evans, M. J., Edwards, P. M., Whalley, L. K., Heard, D. E., Slater, E. J., Woodward-Massey, R., Ye, C., Mehra, A., Worrall, S. D., Bacak, A., Coe, H., Percival, C. J., Hewitt, C. N., Lee, J. D., Cui, T., Surratt, J. D., Wang, X., Lewis, A. C., Rickard, A. R., and Hamilton, J. F.: Low-NO atmospheric oxidation pathways in a polluted megacity, *Atmos. Chem. Phys.*, 21, 1613–1625, <https://doi.org/10.5194/acp-21-1613-2021>, 2021.
- O'Meara, S., Booth, A. M., Barley, M. H., Topping, D., and McFiggans, G.: An assessment of vapour pressure estimation methods, *Phys. Chem. Chem. Phys.*, 16, 19453–19469, <https://doi.org/10.1039/c4cp00857j>, 2014.
- Osthoff, H. D., Sommariva, R., Baynard, T., Pettersson, A., Williams, E. J., Lerner, B. M., Roberts, J. M., Stark, H., Goldan, P. D., Kuster, W. C., Bates, T. S., Coffman, D., Ravishankara, A. R., and Brown, S. S.: Observation of daytime N<sub>2</sub>O<sub>5</sub> in the marine boundary layer during New England Air Quality Study-Intercontinental Transport and Chemical Transformation 2004, *J. Geophys. Res.-Atmos.*, 111, D23S14, <https://doi.org/10.1029/2006jd007593>, 2006.
- Palmer, P. I., Marvin, M. R., Siddans, R., Kerridge, B. J., and Moore, D. P.: Nocturnal survival of isoprene linked to formation of upper tropospheric organic aerosol, *Science*, 375, 562–566, <https://doi.org/10.1126/science.abg4506>, 2022.
- Paulot, F., Crounse, J. D., Kjaergaard, H. G., Kürten, A., St Clair, J. M., Seinfeld, J. H., and Wennberg, P. O.: Unexpected Epoxide Formation in the Gas-Phase Photooxidation of Isoprene, *Science*, 325, 730–733, <https://doi.org/10.1126/science.1172910>, 2009.
- Pfannerstill, E. Y., Reijrink, N. G., Edtbauer, A., Ringsdorf, A., Zannoni, N., Araújo, A., Ditas, F., Holanda, B. A., Sá, M. O., Tsokankunku, A., Walter, D., Wolff, S., Lavrič, J. V., Pöhlker, C., Sörgel, M., and Williams, J.: Total OH reactivity over the Amazon rainforest: variability with temperature, wind, rain, altitude, time of day, season, and an overall budget closure, *Atmos. Chem. Phys.*, 21, 6231–6256, <https://doi.org/10.5194/acp-21-6231-2021>, 2021.
- Pye, H. O., Luecken, D. J., Xu, L., Boyd, C. M., Ng, N. L., Baker, K. R., Ayres, B. R., Bash, J. O., Baumann, K., Carter, W. P., Edgerton, E., Fry, J. L., Hutzell, W. T., Schwede, D. B., and Shepson, P. B.: Modeling the Current and Future Roles of Particulate Organic Nitrates in the Southeastern United States, *Environ. Sci. Technol.*, 49, 14195–14203, <https://doi.org/10.1021/acs.est.5b03738>, 2015.
- Reeves, C. E., Mills, G. P., Whalley, L. K., Acton, W. J. F., Bloss, W. J., Crilley, L. R., Grimmond, S., Heard, D. E., Hewitt, C. N., Hopkins, J. R., Kotthaus, S., Kramer, L. J., Jones, R. L., Lee, J. D., Liu, Y., Ouyang, B., Slater, E., Squires, F., Wang, X., Woodward-Massey, R., and Ye, C.: Observations of speciated isoprene nitrates in Beijing: implications for isoprene chemistry, *Atmos. Chem. Phys.*, 21, 6315–6330, <https://doi.org/10.5194/acp-21-6315-2021>, 2021.
- Ren, J., Hao, Y., Simayi, M., Shi, Y., and Xie, S.: Spatiotemporal variation of surface ozone and its causes in Beijing, China since 2014, *Atmos. Environ.*, 260, 118556, <https://doi.org/10.1016/j.atmosenv.2021.118556>, 2021.
- Schwantes, R. H., Charan, S. M., Bates, K. H., Huang, Y., Nguyen, T. B., Mai, H., Kong, W., Flagan, R. C., and Seinfeld, J. H.: Low-volatility compounds contribute significantly to isoprene secondary organic aerosol (SOA) under high-NO<sub>x</sub> conditions, *Atmos. Chem. Phys.*, 19, 7255–7278, <https://doi.org/10.5194/acp-19-7255-2019>, 2019.
- Schwantes, R. H., Teng, A. P., Nguyen, T. B., Coggon, M. M., Crounse, J. D., St. Clair, J. M., Zhang, X., Schilling, K. A., Seinfeld, J. H., and Wennberg, P. O.: Isoprene NO<sub>3</sub> Oxidation Products from the RO<sub>2</sub> + HO<sub>2</sub> Pathway, *J. Phys. Chem. A*, 119, 10158–10171, <https://doi.org/10.1021/acs.jpca.5b06355>, 2015.
- Schwantes, R. H., Emmons, L. K., Orlando, J. J., Barth, M. C., Tyn-dall, G. S., Hall, S. R., Ullmann, K., St. Clair, J. M., Blake, D. R., Wisthaler, A., and Bui, T. P. V.: Comprehensive isoprene and terpene gas-phase chemistry improves simulated surface ozone in the southeastern US, *Atmos. Chem. Phys.*, 20, 3739–3776, <https://doi.org/10.5194/acp-20-3739-2020>, 2020.
- Shi, Z., Vu, T., Kotthaus, S., Harrison, R. M., Grimmond, S., Yue, S., Zhu, T., Lee, J., Han, Y., Demuzere, M., Dunmore, R. E., Ren, L., Liu, D., Wang, Y., Wild, O., Allan, J., Acton, W. J., Barlow, J., Barratt, B., Beddows, D., Bloss, W. J., Calzolari, G., Carruthers, D., Carslaw, D. C., Chan, Q., Chatzidiakou, L., Chen, Y., Crilley, L., Coe, H., Dai, T., Doherty, R., Duan, F., Fu, P., Ge, B., Ge, M., Guan, D., Hamilton, J. F., He, K., Heal, M., Heard, D., Hewitt, C. N., Holloway, M., Hu, M., Ji, D., Jiang, X., Jones, R., Kalberer, M., Kelly, F. J., Kramer, L., Langford, B., Lin, C., Lewis, A. C., Li, J., Li, W., Liu, H., Liu, J., Loh, M., Lu, K., Lucarelli, F., Mann, G., McFiggans, G., Miller, M. R., Mills, G., Monk, P., Nemitz, E., O'Connor, F., Ouyang, B., Palmer, P. I., Percival, C., Popoola, O., Reeves, C., Rickard, A. R., Shao, L., Shi, G., Spracklen, D., Stevenson, D., Sun, Y., Sun, Z., Tao, S., Tong, S., Wang, Q., Wang, W., Wang, X., Wang, X., Wang, Z., Wei, L., Whalley, L., Wu, X., Wu, Z., Xie, P., Yang, F., Zhang, Q., Zhang, Y., Zhang, Y., and Zheng, M.: Introduction to the special issue “In-depth study of air pollution sources and processes within Beijing and its surrounding region (APHH-Beijing)”, *Atmos. Chem. Phys.*, 19, 7519–7546, <https://doi.org/10.5194/acp-19-7519-2019>, 2019.
- Shrivastava, M., Andreae, M. O., Artaxo, P., Barbosa, H. M. J., Berg, L. K., Brito, J., Ching, J., Easter, R. C., Fan, J., Fast, J. D., Feng, Z., Fuentes, J. D., Glasius, M., Goldstein, A. H., Alves, E. G., Gomes, H., Gu, D., Guenther, A., Jathar, S. H., Kim, S., Liu, Y., Lou, S., Martin, S. T., McNeill, V. F., Medeiros, A., De Sá, S. S., Shilling, J. E., Springston, S. R., Souza, R. A. F., Thornton, J. A., Isaacman-Vanwertz, G., Yee, L. D., Ynoue, R., Zaveri, R. A., Zelenyuk, A., and Zhao, C.: Urban pollution greatly enhances formation of natural aerosols over the Amazon rainforest, *Nat. Commun.*, 10, 1046, <https://doi.org/10.1038/s41467-019-08909-4>, 2019.
- Sommariva, R., Cox, S., Martin, C., Borońska, K., Young, J., Jimack, P. K., Pilling, M. J., Matthaios, V. N., Nelson, B. S., Newland, M. J., Panagi, M., Bloss, W. J., Monks, P. S., and Rickard, A. R.: AtChem (version 1), an open-source box model for the Master Chemical Mechanism, *Geosci. Model Dev.*, 13, 169–183, <https://doi.org/10.5194/gmd-13-169-2020>, 2020.
- Surratt, J. D., Chan, A. W. H., Eddingsaas, N. C., Chan, M., Loza, C. L., Kwan, A. J., Hersey, S. P., Flagan, R. C., Wennberg, P. O., and Seinfeld, J. H.: Reactive intermediates revealed in secondary organic aerosol formation from isoprene, *P. Natl. Acad. Sci. USA*, 107, 6640–6645, <https://doi.org/10.1073/pnas.0911114107>, 2010.

- Topping, D., Barley, M., Bane, M. K., Higham, N., Aumont, B., Dingle, N., and McFiggans, G.: UManSysProp v1.0: an online and open-source facility for molecular property prediction and atmospheric aerosol calculations, *Geosci. Model Dev.*, 9, 899–914, <https://doi.org/10.5194/gmd-9-899-2016>, 2016.
- Tsiligiannis, E., Wu, R., Lee, B. H., Salvador, C. M., Priestley, M., Carlsson, P. T. M., Kang, S., Novelli, A., Vereecken, L., Fuchs, H., Mayhew, A. W., Hamilton, J. F., Edwards, P. M., Fry, J. L., Brownwood, B., Brown, S. S., Wild, R. J., Bannan, T. J., Coe, H., Allan, J., Surratt, J. D., Bacak, A., Artaxo, P., Percival, C., Guo, S., Hu, M., Wang, T., Mentel, T. F., Thornton, J. A., and Halquist, M.: A Four Carbon Organonitrate as a Significant Product of Secondary Isoprene Chemistry, *Geophys. Res. Lett.*, 49, e2021GL097366, <https://doi.org/10.1029/2021gl097366>, 2022.
- Vasquez, K. T., Crounse, J. D., Schulze, B. C., Bates, K. H., Teng, A. P., Xu, L., Allen, H. M., and Wennberg, P. O.: Rapid hydrolysis of tertiary isoprene nitrate efficiently removes NO<sub>x</sub> from the atmosphere, *P. Natl. Acad. Sci. USA*, 117, 33011–33016, <https://doi.org/10.1073/pnas.2017442117>, 2020.
- Vereecken, L. and Nozière, B.: H migration in peroxy radicals under atmospheric conditions, *Atmos. Chem. Phys.*, 20, 7429–7458, <https://doi.org/10.5194/acp-20-7429-2020>, 2020.
- Vereecken, L., Carlsson, P. T. M., Novelli, A., Bernard, F., Brown, S. S., Cho, C., Crowley, J. N., Fuchs, H., Mellouki, W., Reimer, D., Shenolikar, J., Tillmann, R., Zhou, L., Kiendler-Scharr, A., and Wahner, A.: Theoretical and experimental study of peroxy and alkoxy radicals in the NO<sub>3</sub>-initiated oxidation of isoprene, *Phys. Chem. Chem. Phys.*, 23, 5496–5515, <https://doi.org/10.1039/d0cp06267g>, 2021.
- Wang, H., Chen, X., Lu, K., Hu, R., Li, Z., Wang, H., Ma, X., Yang, X., Chen, S., Dong, H., Liu, Y., Fang, X., Zeng, L., Hu, M., and Zhang, Y.: NO<sub>3</sub> and N<sub>2</sub>O<sub>5</sub> chemistry at a suburban site during the EXPLORE-YRD campaign in 2018, *Atmos. Environ.*, 224, 117180, <https://doi.org/10.1016/j.atmosenv.2019.117180>, 2020.
- Wei, W., Li, Y., Ren, Y., Cheng, S., and Han, L.: Sensitivity of summer ozone to precursor emission change over Beijing during 2010–2015: A WRF-Chem modeling study, *Atmos. Environ.*, 218, 116984, <https://doi.org/10.1016/j.atmosenv.2019.116984>, 2019.
- Wennberg, P. O., Bates, K. H., Crounse, J. D., Dodson, L. G., McVay, R. C., Mertens, L. A., Nguyen, T. B., Praske, E., Schwantes, R. H., Smarte, M. D., St Clair, J. M., Teng, A. P., Zhang, X., and Seinfeld, J. H.: Gas-Phase Reactions of Isoprene and Its Major Oxidation Products, *Chem. Rev.*, 118, 3337–3390, <https://doi.org/10.1021/acs.chemrev.7b00439>, 2018.
- Whalley, L. K., Slater, E. J., Woodward-Massey, R., Ye, C., Lee, J. D., Squires, F., Hopkins, J. R., Dunmore, R. E., Shaw, M., Hamilton, J. F., Lewis, A. C., Mehra, A., Worrall, S. D., Bacak, A., Bannan, T. J., Coe, H., Percival, C. J., Ouyang, B., Jones, R. L., Crilley, L. R., Kramer, L. J., Bloss, W. J., Vu, T., Kotthaus, S., Grimmond, S., Sun, Y., Xu, W., Yue, S., Ren, L., Acton, W. J. F., Hewitt, C. N., Wang, X., Fu, P., and Heard, D. E.: Evaluating the sensitivity of radical chemistry and ozone formation to ambient VOCs and NO<sub>x</sub> in Beijing, *Atmos. Chem. Phys.*, 21, 2125–2147, <https://doi.org/10.5194/acp-21-2125-2021>, 2021.
- Williams, J., Keβel, S. U., Nölscher, A. C., Yang, Y., Lee, Y., Yáñez-Serrano, A. M., Wolff, S., Kesselmeier, J., Klüpfel, T., Lelieveld, J., and Shao, M.: Opposite OH reactivity and ozone cycles in the Amazon rainforest and megacity Beijing: Subversion of biospheric oxidant control by anthropogenic emissions, *Atmos. Environ.*, 125, 112–118, <https://doi.org/10.1016/j.atmosenv.2015.11.007>, 2016.
- Xiong, F., McAvey, K. M., Pratt, K. A., Groff, C. J., Hostetler, M. A., Lipton, M. A., Starn, T. K., Seeley, J. V., Bertman, S. B., Teng, A. P., Crounse, J. D., Nguyen, T. B., Wennberg, P. O., Misztal, P. K., Goldstein, A. H., Guenther, A. B., Koss, A. R., Olson, K. F., de Gouw, J. A., Baumann, K., Edgerton, E. S., Feiner, P. A., Zhang, L., Miller, D. O., Brune, W. H., and Shepson, P. B.: Observation of isoprene hydroxynitrates in the southeastern United States and implications for the fate of NO<sub>x</sub>, *Atmos. Chem. Phys.*, 15, 11257–11272, <https://doi.org/10.5194/acp-15-11257-2015>, 2015.
- Xue, L., Gu, R., Wang, T., Wang, X., Saunders, S., Blake, D., Louie, P. K. K., Luk, C. W. Y., Simpson, I., Xu, Z., Wang, Z., Gao, Y., Lee, S., Mellouki, A., and Wang, W.: Oxidative capacity and radical chemistry in the polluted atmosphere of Hong Kong and Pearl River Delta region: analysis of a severe photochemical smog episode, *Atmos. Chem. Phys.*, 16, 9891–9903, <https://doi.org/10.5194/acp-16-9891-2016>, 2016.